CHINESE OPTICS LETTERS

Vol. 21, No. 1 | January 2023

Generation of 12th order harmonic mode-locking in a Nd-doped single-mode all-fiber laser operating at 0.9 μm

Bin Zhang (张 斌)[1], Ping Li (李 平)[1,2], Zhaojun Liu (刘兆军)[1,2], Ming Li (李 明)[2], Jing Liu (刘 靖)[2], Haoxu Zhao (赵浩旭)[2], Qiongyu Hu (胡琼宇)[1], and Xiaohan Chen (陈晓寒)[2*]

[1] Center for Optics Research and Engineering, Key Laboratory of Laser & Infrared System, Ministry of Education, Shandong University, Qingdao 266237, China

[2] School of Information Science and Engineering, Shandong Provincial Key Laboratory of Laser Technology and Application, Shandong University, Qingdao 266237, China

*Corresponding author: cxh@sdu.edu.cn

Received May 17, 2022 | Accepted July 22, 2022 | Posted Online September 22, 2022

Based on the Nd-doped single-mode fiber as the gain medium, an all-fiber 12th harmonic mode-locked (HML) laser operating at the 0.9 μm waveband was obtained for the first time, to the best of our knowledge. A mandrel with a diameter of 10 mm was employed to introduce bending losses to suppress mode competition at 1.06 μm, which resulted in a suppression ratio of up to 54 dB. The 1st–12th order HML pulses with the tunable repetition rate of 494.62 kHz–5.94 MHz were obtained in the mode-locked laser with a center wavelength of ∼904 nm. In addition, the laser has an extremely low threshold pump power of 88 mW. To the best of our knowledge, this is the first time that an HML pulse has been achieved in a 0.9 μm Nd-doped single-mode all-fiber mode-locked laser with the advantages of low cost, simple structure, and compactness, which could be an ideal light source for two-photon microscopy.

Keywords: Nd-doped fiber laser; harmonic mode-locking; bending loss; nonlinear polarization rotation; low repetition rate.
DOI: 10.3788/COL202321.011405

1. Introduction

Pulsed fiber lasers at a low repetition rate on the order of a few megahertz or kilohertz are powerful tools for many research and industrial applications such as material processing, remote sensing, bioscience, and lidar[1–4]. Up to now, Yb, Er, Ho, and Tm-doped fiber lasers with low repetition rate have been widely investigated and have achieved impressive results[5–7]. However, as an indispensable gain ion, Nd-doped lasers are still mainly concentrated in bulk solid-state lasers, and Nd-doped crystals have been extensively employed, such as Nd:$Y_3Al_5O_{12}$ (Nd:YAG), Nd:YVO_4, and Nd:$LiYF_4$ (Nd:YLF)[8]. Pulsed lasers based on Nd-doped fibers have also been reported, but the structure or doped substrates of Nd-doped fibers have been specially designed, such as W-type fibers[9], double-clad fibers[10], microstructured fibers[11], glass fibers[12], and fluorophosphate or phosphate fibers[13]. Moreover, the architectures of the above-mentioned lasers were based on spatial optical paths, and reports of Nd-doped all-fiber mode-locked lasers were relatively scarce[14,15].

Pulsed lasers operating at 0.9 μm have important applications in many fields. Firstly, 0.9 μm mode-locked fiber lasers can be used as the sources for two-photon microscopy (TPM)[16]. For TPM, the best imaging results are obtained in the ∼900 nm band because it corresponds exactly to the excitation wavelength of green fluorescent protein (GFP), which can attach to almost any protein of interest[17]. Secondly, a frequency-doubling 0.9 μm laser can generate a pure blue laser of ∼460 nm, which has great application value in the fields of material processing, optical information storage, and display technology[18]. Further, 0.9 μm mode-locked fiber lasers can be used to generate deep ultraviolet (DUV) at 226 nm after frequency quadrupling[19]. DUV high-energy pulsed lasers with wavelengths less than 250 nm have important values in dermatology, material processing, and laser-induced spectroscopy. Despite its great application potential, research on 0.9 μm Nd-doped fiber lasers has not received much attention. Using the three-level transition of Yb ions, the Yb-doped fiber laser can achieve laser emission in the 980 nm waveband, but it can only generate blue–green light at 490 nm after frequency doubling, which affects the application effect[20]. At present, the tunable Ti:sapphire mode-locked laser can achieve laser emission in the 890–940 nm waveband. However, the disadvantages of high cost, large size, high maintenance cost, and low conversion efficiency greatly limit the application of Ti:sapphire lasers[21]. Fortunately, the Nd ion can achieve laser emission in the 890–940 nm waveband corresponding to the three-level transition of $^4F_{3/2} \rightarrow {}^4I_{9/2}$. However, the Nd-doped all-fiber mode-locked lasers operating at 0.9 μm are rarely reported, and further research is very necessary[14].

In recent years, harmonic mode-locked (HML) lasers have attracted much attention because they can generate pulses with tunable repetition rates[22,23]. A series of HML fiber lasers have been obtained by means of active mode-locking, passive mode-locking, and sub-loops[24–27]. Among them, the passive HML lasers stand out due to their simple structure, low cost, and self-stabilization of repetition frequency. The experimental and theoretical analysis results proved that a necessary condition for obtaining HML operation is that there must be strong nonlinear effects in the cavity, which leads to the generation of multiple pulses[28,29]. Among these multiple pulses, the attractive force between adjacent pulses makes the pulses attract each other to form pulse groups, such as bound-state solitons, pulse bursts, or even soliton rain[30,31]. Conversely, repulsive forces between adjacent pulses will push the pulses away from each other, resulting in uniform or non-uniform pulse distribution throughout the cavity. The generation of HML is closely related to the long-range interaction of multiple pulses in the cavity, including the acoustic-wave effect, dispersive wave, and the gain depletion and recovery mechanisms[32–34]. The establishment process of passive HML has to go through the steps of the birth of a giant pulse, instability caused by self-phase modulation, pulse splitting, repulsion and separation of multiple pulses, etc., and finally a stable HML pulse is formed[35]. It can be seen that pulse splitting is an essential part of the whole process. However, without pulse splitting, the dissipative soliton energies obtainable in the all-normal dispersion cavity are much higher than the self-similar pulse energy obtainable in the dispersion management cavity and the traditional soliton energy obtainable in the all-negative dispersion cavity[36]. Therefore, it is more difficult to obtain HML operations in an all-normal dispersion cavity. At the 0.9 μm waveband, the optical fiber devices are all in the positive dispersion region. So far, to our knowledge, there has been no report of an HML laser operating at the 0.9 μm waveband.

In this paper, based on the Nd-doped single-mode fiber (SMF) as the gain medium and nonlinear polarization rotation (NPR) as the saturable absorber (SA), an all-fiber 12th order HML laser operating at the 0.9 μm waveband was realized for the first time, to the best of our knowledge. Bending losses were introduced through a mandrel with a diameter of 10 mm to suppress stimulated emission at 1.06 μm, resulting in a suppression ratio of 0.9 versus 1.06 μm up to 54 dB. Fundamental frequencies of ~12th order HML pulses with the tunable repetition rate of 494.62 kHz–5.94 MHz were obtained in the mode-locked laser with a center wavelength of ~904 nm. In addition, the laser has an extremely low threshold pump power of 88 mW. To the best of our knowledge, a 0.9 μm Nd-doped all-fiber HML laser has been obtained for the first time, which can enable a portable 0.9 μm HML laser with tunable repetition rate. The 0.9 μm HML laser can be used in TPM to improve imaging quality.

2. Experimental Setup

The experimental configuration of NPR mode-locking Nd-doped single-mode all-fiber HML laser is shown in Fig. 1.

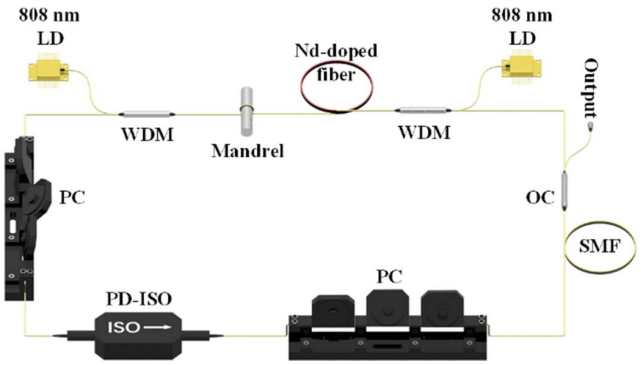

Fig. 1. Experimental setup of the NPR mode-locking Nd-doped single-mode all-fiber HML laser based on bending loss.

To obtain sufficiently strong nonlinear effects in the cavity, two 808 nm wavelength-locked single-mode laser diodes (LDs, Lumics) with a maximum pump power of 200 mW were used as the pump source. Two WDMs were used to direct the pump light of the two LDs into the ring cavity to form a double-ended pump. The gain medium in the cavity adopted a 2.75 m Nd-doped SMF (CorActive, Nd-103) with a numerical aperture of 0.14, core diameter of 4.5 μm, peak absorption of 37 dB/m around 805 nm, and group velocity dispersion (GVD) at 910 nm of 39.21 ps^2/km. The SMF behind the Nd-doped fiber was wound around a mandrel with a diameter of 10 mm for one turn to introduce bending losses. Two polarization controllers (PCs) were employed to regulate the polarization state of the cavity, and a polarization-dependent isolator (PD-ISO) with a center wavelength of 910 nm was used for ensuring the unidirectional transmission of light in the cavity and acting as a polarizer. Mode-locked pulses were extracted from the 10% port of a 10:90 fiber coupler (OC) with a center wavelength of 910 nm. In order to obtain HML operation, an indispensable condition is that there must be strong nonlinear effects in the cavity, which can be achieved by increasing the pump power or lengthening the fiber. However, when the pump power is limited to 400 mW, the intracavity nonlinear effect can be enhanced by lengthening the fiber. For this purpose, a piece of ~410 m SMF (Nufern, 780-HP) with GVD of 32.97 ps^2/km at 910 nm was inserted into the cavity. The total length of the ring cavity was approximately 417.83 m, corresponding to net all-normal dispersion of 13.79 ps^2.

3. Results and Discussion

There are some challenges in obtaining a Nd-doped all-fiber mode-locked laser operating at 0.9 μm. On the one hand, the emission cross section of the Nd-doped fiber is an order of magnitude higher at 1.06 μm than at 0.9 μm. On the other hand, the emission at 0.9 μm of the Nd-doped fiber corresponds to a quasi-three-level $^4F_{3/2} \rightarrow {}^4I_{9/2}$ transition, while the 1.06 μm Nd-doped fiber laser belongs to a four-level laser system. As we all know, the three-level laser system naturally has a higher threshold than the four-level laser system. Therefore, in order to realize the

Nd-doped fiber mode-locked laser operating at 0.9 μm, a method to suppress the emission of Nd-doped fiber at 1.06 μm should be implemented. For this purpose, a series of measures have been proposed. Cook *et al.* pointed out that the operating efficiency of the three-level system can be improved by doping the Nd-doped fiber with special ions, such as aluminum ions or germanium ions[37]. In addition, the suppression of the four-level laser system can also be realized by special design of the structure of the Nd-doped fiber, such as photonic crystal bandgap fiber or W-type double-clad Nd-doped fiber[9–11]. In 2021, Corre *et al.* demonstrated for the first time, to the best of our knowledge, an all-polarization-maintaining (PM) Nd-doped fiber mode-locked laser near 910 nm based on a semiconductor SA mirror (SESAM) as an SA[38]. Recently, using the Nd-doped PM fiber as the gain medium, a 0.9 μm Nd-doped all-fiber mode-locked laser based on the nonlinear amplifying loop mirror (NALM) has been demonstrated for the first time, to the best of our knowledge, by Mkrtchyan *et al.*[14]. To suppress dominant emission at 1064 nm, a 920/1064 nm wavelength division multiplexer (WDM) was inserted into the cavity as a filter. However, both the W-type double-clad and the PM Nd-doped fiber have some disadvantages compared with Nd-doped SMF, such as difficulty in drawing and high cost. Moreover, the cost of the laser was bound to be further increased by adding components such as WDM and filters into the cavity. Therefore, other schemes to suppress the emission at 1.06 μm should be considered in order to obtain a low-cost 0.9 μm Nd-doped all-fiber mode-locked laser.

The bending loss of SMF increases with a decreasing radius of curvature. At the same time, the bending loss also increases as the operating wavelength increases, that is, for the same bending radius, the light with longer wavelength will experience greater losses[39]. Therefore, compared with 0.9 μm, the light of 1.06 μm has a larger bending loss, which can be used to suppress the stimulated emission of Nd-doped fibers at 1.06 μm. Firstly, an optimal bend radius should be found that does not affect the performance of the laser operating at 0.9 μm, but completely suppresses the emission of the Nd-doped fiber at 1.06 μm. For this purpose, as shown in Fig. 2(a), after splicing a section of SMF to the Nd-doped fiber and bending the SMF to different diameters, the emission spectrum of the Nd-doped fiber was measured with an optical spectrum analyzer (Anritsu, MS9740B). As shown in the results in Fig. 2(b), without bending loss, the emission spectrum of the Nd-doped fiber was strongest at 1.06 μm, an order of magnitude smaller at 0.9 μm than 1.06 μm, and weakest at 1.34 μm. This was the reason why a Nd-doped fiber laser operating at 0.9 μm was difficult to achieve. As for the SMF with a bending diameter of 25 mm, the emission of the Nd-doped fiber at 1.34 μm was completely suppressed, while the other two wavebands were hardly affected. When the bending diameter of the SMF was reduced to 12 mm, the emission intensity of the Nd-doped fiber decreased at 1.06 μm, but was still 12 dB higher than that at 0.9 μm, and it is difficult to obtain the ideal suppression effect at this time. The best results were obtained when the SMF has a bending diameter of 10 mm, which can effectively suppress the emission at 1.06 μm without affecting the emission spectrum

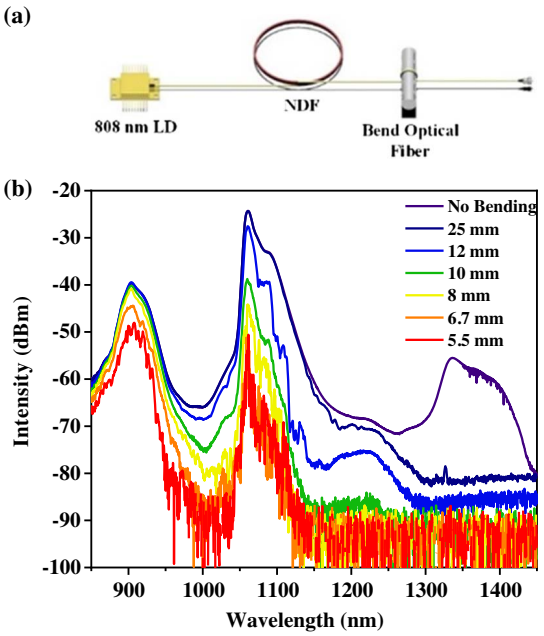

Fig. 2. (a) Simple experimental setup for measuring the emission spectrum of Nd-doped fiber after bending the SMF. (b) Emission spectra of the Nd-doped SMF after bending the SMF with different diameters.

at 0.9 μm. At this time, combined with the filtering effect of other devices with the working wavelength of 0.9 μm in the cavity, the performance of the Nd-doped fiber laser operating at 0.9 μm will be optimized. If the bending diameter of the SMF was further reduced, the emission of the Nd-doped fiber at 0.9 μm will be decreased, which will be detrimental to the performance of the laser. Therefore, in this paper, the optimal bending diameter was chosen to be 10 mm, which can completely suppress the mode competition at 1.06 μm without affecting the performance of the 0.9 μm Nd-doped fiber mode-locked laser.

Then, according to the experimental setup shown in Fig. 1, we built a Nd-doped all-fiber HML laser operating at 0.9 μm. In the experiments, increasing the pump power of LDs to 391 mW and carefully tuning the PC state, a stable 12th HML laser could be recorded. Figure 3(a) presents the emission spectrum of the 12th HML laser over a wide range (860–1150 nm). The central wavelength of laser was 904.31 nm with a 3 dB bandwidth of 2.06 nm. We can see that the emission of the Nd-doped fiber at 1.06 μm has been completely suppressed, and a suppression ratio of 0.9 μm versus 1.06 μm as high as 54 dB has been recorded.

Then, by fixing the state of the PCs and gradually reducing the pump power, the order of the HML decreases gradually. When the pump power was reduced to 136 mW, a mode-locked laser operating at the fundamental frequency was obtained. Figure 3(b) depicts the spectrogram of the laser in a narrow range (860–1000 nm) at this time. Due to the addition of ~410 m SMF in the cavity, this inevitably causes the stimulated Raman scattering (SRS) effect. It can be seen that in addition to the fundamental wave with a central wavelength of 909.84 nm, due to the existence of the SRS effect, the Stokes wave with a

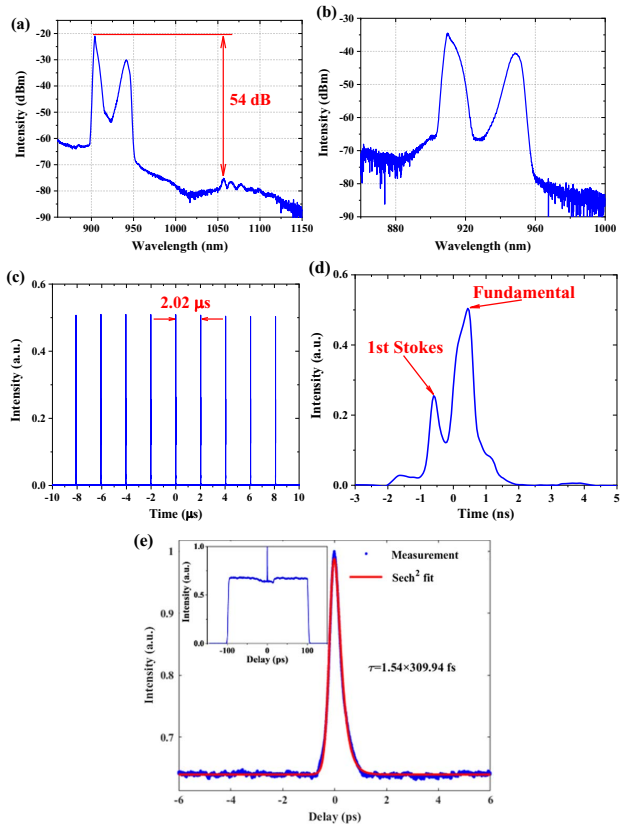

Fig. 3. (a) Emission spectrum of the 12th HML laser over a wide range (860–1150 nm) with a resolution of 0.07 nm. The output characteristics of 0.9 μm Nd-doped all-fiber mode-locked laser operating at the fundamental frequency under the pump power of 136 mW. (b) Emission spectrum. (c) Pulse train. (d) Single-pulse shape. (e) The autocorrelation trace of the coherence spike and its sech^2 fitting within a narrower scan range. Inset: measured autocorrelation trace of the mode-locked pulse within a wider scan range.

central wavelength of 948.34 nm was also recorded. The separation between the two wavelengths was about 436.20 cm^{-1}, which is consistent with the Raman frequency shift of the silica fiber[40]. The pulse characteristics of the mode-locked laser were measured by an ultra-high-speed InGaAs PIN photodetector (EOT, ET-3500 F) with risetime/falltime of < 25 ps combined with a digital oscilloscope (Tektronix, MSO64) with a bandwidth of 4 GHz and sample rate of 25 GS/s. The pulse train and single-pulse shape are shown in Figs. 3(c) and 3(d), respectively. The pulse intensities in the pulse train were nearly constant with a pulse interval of 2.02 μs, corresponding to the cavity round-trip time. Figure 3(d) demonstrates the single-pulse shape with the fine structure of the mode-locked laser. It can be seen that the single-pulse shape contained two peaks with a time interval of about 1040 ps, which is in good agreement with the theoretical time interval of 1079.55 ps calculated from the intracavity dispersion value and the cavity length. The Raman pulse noise is ascribed to the fact that it starts from spontaneous emission reaching high energy after only one round trip of the pump[41,42]. That is, the evolution result of Raman pulse in the cavity without feedback proves that the Raman pulse is only generated in the current cycle and does not participate in the next cycle. Because of the difference in group velocities, afterward, the Raman pulse runs away from the pump pulse[41–43]. It is well known that light with a longer wavelength has a slower transmission speed in an all-normal dispersion environment. The difference in transmission speed will cause the fundamental and Stokes waves to gradually separate in the time domain[43]. Finally, the pulse peak corresponding to the Stokes wave was located at the leading edge of the single-pulse shape, and the pulse peak corresponding to the fundamental wave was located at the back edge of the single-pulse shape, as marked in Fig. 3(d). In terms of intensity, the intensity of the pulse peak corresponding to the first Stokes wave was smaller than the intensity of the pulse peak corresponding to the fundamental wave, which also corresponded to the difference in intensities of the two wavelengths in the spectrum. Then, the autocorrelation trace of the Nd-doped all-fiber mode-locked laser operating at the fundamental frequency was measured with an autocorrelator (Femtochrome, FR-103XL), and the results are presented in Fig. 3(e). The autocorrelation trace within a wider scan range displayed in the inset of Fig. 3(e) showed that a narrower coherence peak was located on a wide and smooth pedestal, which means that a typical noise-like pulse (NLP) autocorrelation trace has been obtained in the experiment. The width of the base of the autocorrelation curve was ~200 ps, corresponding to the measurement range of the autocorrelator. The autocorrelation curve of the coherence spike and its sech^2 fitting within a narrower span range of ±6 ps are plotted in Fig. 3(e). The full width at half-maximum (FWHM) was about 478.30 fs, meaning that the actual pulse duration was about $478.30\ \text{fs} \times 0.648 = 309.94\ \text{fs}$. The reason why the pulses are NLP was mainly due to the existence of the SRS effect, and there have been many previous reports that NLPs were obtained in the Raman mode-locked lasers[44,45].

As the pump power decreased from 391 mW to 88 mW, the order of the HML laser also gradually reduced. Figure 4 depicts the changes in the emission spectra and pulse trains of the HML laser throughout the process. As shown in the change of the spectra in Fig. 4(a), the intensities of both the first Stokes and the fundamental waves decreased with decreasing pump power. The central wavelength of fundamental and first Stokes waves showed a trend of "blue-shift" as the pump power increases. When the pump power was increased to maximum pump power of 391 mW, the central wavelengths of the fundamental and first Stokes waves were 904.38 and 941.55 nm, respectively. Since the emission of the Nd-doped fiber at 0.9 μm corresponds to a quasi-three-level transition, the reabsorption effect of rare-earth (RE) ions can be used to explain the blue-shift of the wave with increasing pump power[46,47]. Since the reabsorption effect of RE ions at long wavelengths was stronger, when the pump power increased, the gain at the long wavelength decreased more drastically. As a result, the center wavelength of the laser was shifted to the short wavelength[48].

With the pump power change, the variation of the pulse trains measured with the high-speed detector is plotted in Fig. 4(b).

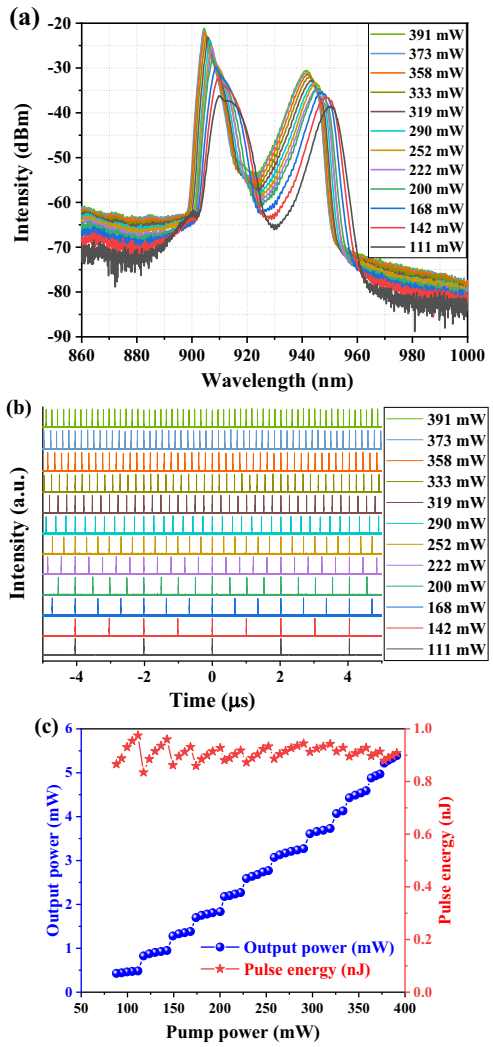

Fig. 4. Evolutions of 0.9 μm Nd-doped all-fiber HML laser when the pump power changed from 88 to 391 mW. (a) Emission spectra. (b) Pulse trains. (c) Average output power and single-pulse energy.

Firstly, in the time domain, as the pump power increases, the number of pulses in a fixed time range gradually increases, and the interval between the adjacent pulses gradually decreases. That is, the pulses are uniformly distributed, and the repetition frequency of the pulses is gradually increased. Meanwhile, although the number of pulses increases with increasing pump power, the peak intensity of the pulses remains almost constant throughout the process. At a certain pump power, the pulse intensities in the pulse train are almost the same, proving that the laser works in a stable state. These phenomena are typical for HML lasers, and it is demonstrated that a stable HML operation has been obtained in our experiments. The order of HML increased with the increase of pump power, and the pulse sequence diagram under each order is shown in Fig. 4(b). Up to 12th HML operation has been obtained under a maximum pump power of 391 mW.

An optical power meter (OPHIR, PD300-IR) was utilized to record the average output power of the HML laser. The dependence of average output power and single-pulse energy on the pump power is presented in Fig. 4(c), and the threshold power of the mode-locked laser was as low as 88 mW. To our knowledge, the threshold of our laser is the lowest among Nd-doped fiber mode-locked lasers operating at 0.9 μm reported so far. The maximum average output power of 5.39 mW was obtained under pumped powers of 391 mW, corresponding to the optical-to-optical conversion efficiency of 1.37%. The trend of the single-pulse energy of the HML laser as a function of the pump power is shown by the red star in Fig. 4(c). It can be seen that under a certain order of HML, the single-pulse energy increased with the increase of the average output power. If the pump power increases, the harmonic mode-locking order increases by one order, the single-pulse energy will drop sharply and then increase with the increase of the output power, and so on. However, the variation of single-pulse energy was within a small range (0.84–0.97 nJ), which can be considered to remain almost unchanged at 0.91 nJ.

In order to analyze the stability of the mode-locked laser, we measured the RF spectra of the 1st, 4th, 8th, and 12th HML

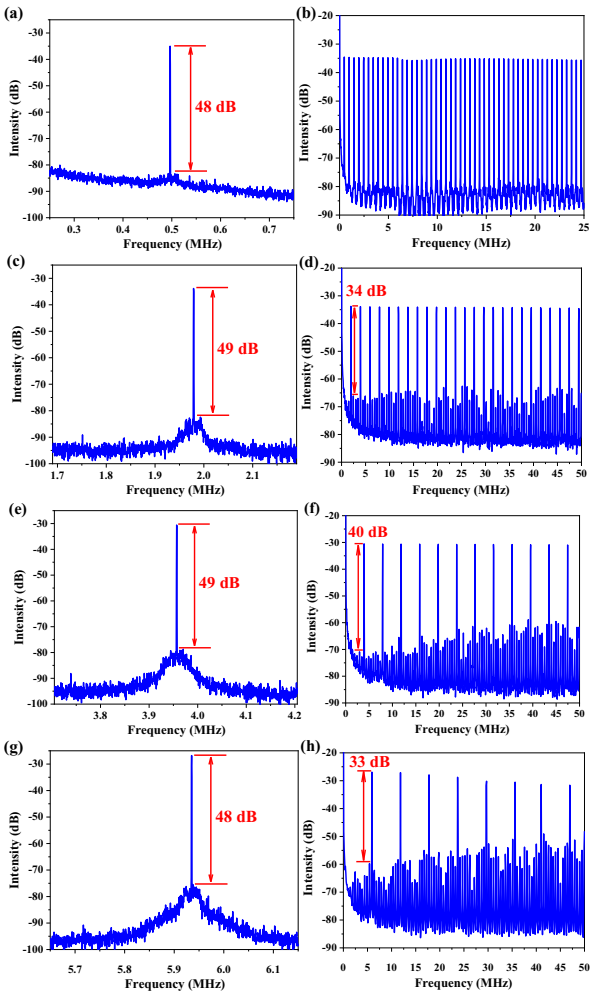

Fig. 5. RF spectra of the 1st, 4th, 8th, and 12th HML laser within different bandwidths.

pulses with a spectrum analyzer (R&S, FPC1000), and the results are shown in Fig. 5. First, at the pump power of 111 mW, the laser operates at the fundamental frequency, and the RF spectrum within a narrow bandwidth of 500 kHz with a resolution of 300 Hz is recorded in Fig. 5(a). It can be seen that the central frequency was located at the fundamental repetition rate of 495 kHz with a signal-to-noise ratio (SNR) higher than 48 dB.

Figure 5(b) illustrates the broadband RF spectrum of the mode-locked laser operating at a fundamental frequency with a bandwidth of 25 MHz and a resolution of 3 kHz, which also exhibits high SNR. As the pump power increases, the mode-locked laser will enter an HML state. Figures 5(c) and 5(d) depict the RF spectra of the fourth HML laser within a narrow bandwidth range of 500 kHz and a bandwidth of 50 MHz, respectively. At this time, the repetition rate of the pulses was 1.98 MHz, the SNR was greater than 49 dB, and the supermode suppression ratio (SMSR) was greater than 34 dB, indicating a stable and low-noise operating status. Additionally, Figs. 5(e) and 5(f) illustrate RF spectra of the eighth HML laser. The repetition rate was measured to be 3.96 MHz, and the SNR and SMSR were suppressed better than 49 dB and 40 dB, respectively. Finally, when the pump power was 391 mW, the highest 12th order HML was obtained, and its RF spectra are shown in Figs. 5(g) and 5(h). The repetition rate of the pulses was located at 5.94 MHz, and the SNR and SMSR were greater than 48 dB and 33 dB, respectively. In general, the narrowband RF spectra of the HML laser under any pump power have an SNR greater than 48 dB, indicating that the laser has been working in a stable state and has strong robustness.

4. Conclusions

In conclusion, we reported for the first time, to the best of our knowledge, a Nd-doped single-mode all-fiber 12th order HML laser operating at the 0.9 μm waveband. We innovatively propose that the emission of the Nd-doped fiber at 1.06 μm can be effectively suppressed by the bending loss of the SMF. To find the optimal bend diameter, we measured the emission spectra of a Nd-doped fiber after splicing a piece of SMF with different bend diameters. A mandrel with a diameter of 10 mm was employed, and a suppression ratio of 0.9 μm versus 1.06 μm of up to 54 dB was achieved. To enhance the nonlinear effect in the cavity, a piece of ∼410 m SMF was inserted into the ring cavity. Under the pump power of 391 mW, we obtained the highest 12th order HML pulse in the Nd-doped all-fiber laser with the fundamental wavelength of 904.38 nm. Then, we investigated the evolutions of emission spectra and pulse trains as a function of pump power. Fundamental frequencies of the ∼12th order HML pulses with the tunable repetition rate of 494.62 kHz–5.94 MHz were obtained in the mode-locked laser. In addition, the laser has an extremely low threshold pump power of 88 mW. It is necessary to point out that, limited by the pump power, only the 12th order HML was obtained in the experiment. But, to the best of our knowledge, our experimental results demonstrated for the first time that the HML can be achieved in a 0.9 μm Nd-doped all-fiber mode-locked laser. We believed that the order of the HML laser will be further improved if higher pump powers are available in the future, which could be an effective source for TPM to improve the imaging effect.

Acknowledgement

This work was supported by the Natural Science Foundation of Shandong Province (Nos. ZR2019MF047, ZR2020MF126, and ZR2019MF043).

References

1. T. Suedmeyer, S. V. Marchese, S. Hashimoto, C. R. E. Baer, G. Gingras, B. Witzel, and U. Keller, "Femtosecond laser oscillators for high-field science," Nat. Photonics **2**, 599 (2008).
2. U. Sharma, E. W. Chang, and S. H. Yun, "Long-wavelength optical coherence tomography at 1.7 μm for enhanced imaging depth," Opt. Express **16**, 19712 (2008).
3. V. Philippov, C. Codemard, Y. Jeong, C. Alegria, J. K. Sahu, J. Nilsson, and G. N. Pearson, "High-energy in-fiber pulse amplification for coherent lidar applications," Opt. Lett. **29**, 2590 (2004).
4. M. Krebs, S. Haedrich, S. Demmler, J. Rothhardt, A. Zair, L. Chipperfield, J. Limpert, and A. Tuennermann, "Towards isolated attosecond pulses at megahertz repetition rates," Nat. Photonics **7**, 555 (2013).
5. M. Mueller, C. Aleshire, A. Klenke, E. Haddad, F. Legare, A. Tuennermann, and J. Limpert, "10.4 kW coherently combined ultrafast fiber laser," Opt. Lett. **45**, 3083 (2020).
6. L.-M. Yang, P. Wan, V. Protopopov, and J. Liu, "2 μm femtosecond fiber laser at low repetition rate and high pulse energy," Opt. Express **20**, 5683 (2012).
7. S. Yang and Y. Qi, "Sub-nanosecond multiple-wavelength harmonic mode-locked Tm-Ho co-doped fiber laser," Opt. Laser Technol. **127**, 106160 (2020).
8. A. Ikesue and Y. L. Aung, "Synthesis and performance of advanced ceramic lasers," J. Am. Ceram. Soc. **89**, 1936 (2006).
9. K. Qian, H. Wang, M. Laroche, and A. Hideur, "Mode-locked Nd-doped fiber laser at 930 nm," Opt. Lett. **39**, 267 (2014).
10. R. Becheker, M. Tang, M. Touil, T. Robin, B. Cadier, M. Laroche, T. Godin, and A. Hideur, "Dissipative soliton resonance in a mode-locked Nd-fiber laser operating at 927 nm," Opt. Lett. **44**, 5497 (2019).
11. A. Wang, A. K. George, and J. C. Knight, "Three-level neodymium fiber laser incorporating photonic bandgap fiber," Opt. Lett. **31**, 1388 (2006).
12. Y. Wang, Y. Zhang, J. Cao, L. Wang, X. Peng, J. Zhong, C. Yang, S. Xu, Z. Yang, and M. Peng, "915 nm all-fiber laser based on novel Nd-doped high alumina and yttria glass @ silica glass hybrid fiber for the pure blue fiber laser," Opt. Lett. **44**, 2153 (2019).
13. G. Zhang, M. Wang, C. Yu, Q. Zhou, J. Qiu, L. Hu, and D. Chen, "Efficient generation of watt-level output from short-length Nd-doped phosphate fiber lasers," IEEE Photon. Technol. Lett. **23**, 350 (2011).
14. A. A. Mkrtchyan, Y. G. Gladush, M. A. Melkumov, A. M. Khegai, K. A. Sitnik, P. G. Lagoudakis, and A. G. Nasibulin, "Nd-doped polarization maintaining all-fiber laser with dissipative soliton resonance mode-locking at 905 nm," J. Light. Technol. **39**, 5582 (2021).
15. B. Zhang, X. Chen, M. Li, H. Zhang, L. Xu, Q. Hu, J. Liu, and P. Li, "Single- and dual-wavelength noise-like pulses generation in a Nd-doped all-fiber ring laser based on nonlinear polarization rotation," Infrared Phys. Technol. **116**, 103744 (2021).
16. F. Helmchen and W. Denk, "Deep tissue two-photon microscopy," Nat. Methods **2**, 932 (2005).
17. J. Lippincott-Schwartz, N. Altan-Bonnet, and G. H. Patterson, "Photobleaching and photoactivation: following protein dynamics in living cells," Nat. Cell Biol. **Suppl**, S7 (2003).
18. C. Bartolacci, M. Laroche, H. Gilles, S. Girard, T. Robin, and B. Cadier, "Generation of picosecond blue light pulses at 464 nm by frequency doubling

an Nd-doped fiber based master oscillator power amplifier," Opt. Express **18**, 5100 (2010).
19. K. L. Corre, T. Robin, A. Barnini, L. Kervella, P. Guitton, B. Cadier, G. Santarelli, H. Gilles, S. Girard, and M. Laroche, "Linearly-polarized pulsed Nd-doped fiber MOPA at 905 nm and frequency conversion to deep-UV at 226 nm," Opt. Express **29**, 4240 (2021).
20. A. Bouchier, G. Lucas-Leclin, P. Georges, and J. M. Maillard, "Frequency doubling of an efficient continuous wave single-mode Yb-doped fiber laser at 978 nm in a periodically-poled MgO:$LiNbO_3$ waveguide," Opt. Express **13**, 6974 (2005).
21. E. Riedle, M. Beutter, S. Lochbrunner, J. Piel, S. Schenkl, S. Sporlein, and W. Zinth, "Generation of 10 to 50 fs pulses tunable through all of the visible and the NIR," Appl. Phys. **71**, 457 (2000).
22. M. Pang, W. He, X. Jiang, and P. S. J. Russell, "All-optical bit storage in a fibre laser by optomechanically bound states of solitons," Nat. Photonics **10**, 454 (2016).
23. N. Tarasov, A. M. Perego, D. V. Churkin, K. Staliunas, and S. K. Turitsyn, "Mode-locking via dissipative Faraday instability," Nat. Commun. **7**, 12441 (2016).
24. H. Chen, S.-P. Chen, Z.-F. Jiang, and J. Hou, "Versatile long cavity widely tunable pulsed Yb-doped fiber laser with up to 27655th harmonic mode locking order," Opt. Express **23**, 1308 (2015).
25. Y. Wang, S. Y. Set, and S. Yamashita, "Active mode-locking via pump modulation in a Tm-doped fiber laser," APL Photonics **1**, 71303 (2016).
26. Q. Hu, X. Zhang, Z. Liu, P. Li, M. Li, Z. Cong, Z. Qin, and X. Chen, "High-order harmonic mode-locked Yb-doped fiber laser based on a $SnSe_2$ saturable absorber," Opt. Laser Technol. **119**, 105639 (2019).
27. R. Wang, L. Jin, J. Wang, S. Xie, X. Li, Y. Xu, H. Zhang, X. Zhao, and X. Ma, "Harmonic mode-locked fiber laser based on microfiber-assisted nonlinear multimode interference," Chin. Opt. Lett. **20**, 010601 (2022).
28. D. R. Solli, G. Herink, B. Jalali, and C. Ropers, "Fluctuations and correlations in modulation instability," Nat. Photonics **6**, 463 (2012).
29. M. Narhi, B. Wetzel, C. Billet, S. Toenger, T. Sylvestre, J.-M. Merolla, R. Morandotti, F. Dias, G. Genty, and J. M. Dudley, "Real-time measurements of spontaneous breathers and rogue wave events in optical fibre modulation instability," Nat. Commun. **7**, 13675 (2016).
30. K. Sulimany, O. Lib, G. Masri, A. Klein, M. Fridman, P. Grelu, O. Gat, and H. Steinberg, "Bidirectional soliton rain dynamics induced by Casimir-like interactions in a graphene mode-locked fiber laser," Phys. Rev. Lett. **121**, 133902 (2018).
31. P. Grelu and J. M. Soto-Crespo, "Multisoliton states and pulse fragmentation in a passively mode-locked fibre laser," J. Opt. B **6**, S271 (2004).
32. A. B. Grudinin and S. Gray, "Passive harmonic mode locking in soliton fiber lasers," J. Opt. Soc. Am. B **14**, 144 (1997).
33. J. M. Soto-Crespo, N. Akhmediev, P. Grelu, and F. Belhache, "Quantized separations of phase-locked soliton pairs in fiber lasers," Opt. Lett. **28**, 1757 (2003).
34. R. Weill, A. Bekker, V. Smulakovsky, B. Fischer, and O. Gat, "Noise-mediated Casimir-like pulse interaction mechanism in lasers," Optica **3**, 189 (2016).
35. X. Liu and M. Pang, "Revealing the buildup dynamics of harmonic mode-locking states in ultrafast lasers," Laser Photon. Rev. **13**, 1800333 (2019).
36. P. Grelu and N. Akhmediev, "Dissipative solitons for mode-locked lasers," Nat. Photonics **6**, 84 (2012).
37. A. L. Cook and H. D. Hendricks, "Diode-laser-pumped tunable 896-939.5-nm neodymium-doped fiber laser with 43-mW output power," Appl. Opt. **37**, 3276 (1998).
38. K. Le Corre, T. Robin, B. Cadier, R. Becheker, T. Godin, A. Hideur, H. Gilles, S. Girard, and M. Laroche, "Mode-locked all-PM Nd-doped fiber laser near 910 nm," Opt. Lett. **46**, 3564 (2021).
39. W. Gambling, H. Matsumura, and C. Ragdale, "Curvature and microbending losses in single-mode optical fibers," Opt. Quantum Electron. **11**, 43 (1979).
40. R. H. Stolen, C. Lee, and R. K. Jain, "Development of the stimulated Raman spectrum in single-mode silica fibers," J. Opt. Soc. Am. B **1**, 652 (1984).
41. S. A. Babin, E. V. Podivilov, D. S. Kharenko, A. E. Bednyakova, M. P. Fedoruk, V. L. Kalashnikov, and A. Apolonski, "Multicolour nonlinearly bound chirped dissipative solitons," Nat. Commun. **5**, 4653 (2014).
42. A. E. Bednyakova, S. A. Babin, D. S. Kharenko, E. V. Podivilov, M. P. Fedoruk, V. L. Kalashnikov, and A. Apolonski, "Evolution of dissipative solitons in a fiber laser oscillator in the presence of strong Raman scattering," Opt. Express **21**, 20556 (2013).
43. G. P. Agrawal, *Nonlinear Fiber Optics*, 6th ed. (Academic, 2019).
44. W.-C. Chang, J.-H. Lin, T.-Y. Liao, and C.-Y. Yang, "Characteristics of noise-like pulse with broad bandwidth based on cascaded Raman scattering," Opt. Express **26**, 31808 (2018).
45. J.-H. Lin, T.-Y. Liao, C.-Y. Yang, D.-G. Zhang, C.-Y. Yang, Y.-W. Lee, S. Das, A. Dhar, and M. C. Paul, "Noise-like pulse generation around 1.3-μm based on cascaded Raman scattering," Opt. Express **28**, 12252 (2020).
46. B. Zhang, X. Chen, X. Zhang, Z. Liu, M. Li, J. Liu, L. Xu, Q. Hu, and P. Li, "Unusual evolutions of pulses and spectra in an Yb-doped intra-cavity cascaded Raman fiber laser," Infrared Phys. Technol. **120**, 103990 (2022).
47. H. Yu, X. Wang, P. Zhou, X. Xu, and J. Chen, "Raman continuum generation at 1.0–1.3 μm in passively mode-locked fiber laser based on nonlinear polarization rotation," Appl. Phys. B **117**, 305 (2014).
48. D. J. Richardson, J. Nilsson, and W. A. Clarkson, "High power fiber lasers: current status and future perspectives," J. Opt. Soc. Am. B **27**, B63 (2010).